Nonlinear and Nonparallel Receptivity of Zero-pressure Gradient Boundary Layer

Tapan K. Sengupta, Swagata Bhaumik, Vikram Singh, Sarvagy Shukl
Department of Aerospace Engineering, I.I.T. Kanpur, U.P. 208016, India;
e-mail: tksen@iitk.ac.in,

ABSTRACT

Nonlinear and nonparallel receptivity of zero pressure gradient boundary layer have been investigated by solving the full two-dimensional Navier-Stokes equation with respect to wall excitation at fixed frequency. The excitation is triggered through a blowing-suction strip at a location near the leading edge of the plate. Results are reported for cases which are linearly stable in a spatial formulation, for different amplitudes of the excitation of the strip.

Presented results for a lower amplitude of excitation for the chosen frequency of excitation help explain the displayed nonlinearity of the streamwise component of the disturbance velocity at intermediate heights inside the shear layer. The disturbance field is noted to be neutrally stable at heights close to the plate and in the outer part of the boundary layer. Overall, such behaviour of the disturbance field is explained in terms of the presence of multiple modes and their spatiotemporal interactions and the importance of nonlinearity at specific heights inside the shear layer. We report another case where stationary bubbles are formed at the wall near the exciter, when the amplitude of excitation is doubled over previous lower amplitude case. Presence of such bubbles alter the disturbance growth significantly and is an early marker of bypass transition.

Key Words: Nonlinear Receptivity; Nonparallel effects; Navier-Stokes equation; Orr-Sommerfeld Equation; Bypass Transition; Tollmien-Schlighting Waves

1. INTRODUCTION

Significant progress in the understanding of flow instability has been made over the last few decades starting with the original works reported in Heisenberg [1], Tollmien [2] and Schlichting [3] that theoretically established the process of flow transition from laminar to turbulent state to follow with the creation and growth of waves (now known as Tollmien-Schlichting (TS) waves). The latter nomenclature is a misnomer as under the guidance of Sommerfield, Heisenberg studied this flow for his doctoral dissertation. His committee could find nothing wrong in the analysis, but found it difficult to accept that viscous action can add to instability. Of course, it makes perfect sense when one realizes that viscous action sets a phase delay that can lead to positive feedback and instability. Thus, the credit for the original observation of the existence of viscous tuned instability waves should be conferred equally to Heisenberg, Tollmien and Schlichting.

These theoretical results were obtained with restrictive assumptions on the growth of the equilibrium flow whose stability was studied in a linear framework. These two restrictions cause error due to what is known as non-inclusion of nonlinearity and non-parallelism. While these two neglected effects are still the subject of many investigations- including the present one- the major issue of concern in accepting the results of Tollmien [2] and Schlichting [3] were due to the challenge that these studies posed to contemporary paradigmatic acceptance of the fact that viscous effects can only be stabilizing. The latter point of view was based on the pioneering work done in this field earlier by Kelvin [4] and Rayleigh [5,6] that was premised on the assumption that viscous action being dissipative in fluid flow, its inclusion was not essential for the study of flow instability. Specifically, Rayleigh [5,6] propounded a criterion that determined the inviscid instability of shear layers. In contrast to this, the work reported in Tollmien [2] and Schlichting [3] stated that the complex interactions of viscous action along with inertial terms of the governing equation can actually destabilize a flow that was otherwise pronounced as stable. A typical example of such a flow is the zero pressure gradient boundary layer developing over a flat plate. Apart from the problem of countering the prevalent idea of flow instability, the predicted TS waves were not seen experimentally till the results of Schubauer & Skramstad [7] were published.

Earlier experimental results were bedevilled due to the experimental device noise and in the design of appropriate experiment that follows the conceptual construct of the theoretical formulation. This last aspect relates to the eigenvalue problem in Tollmien [2] and Schlichting [3] that discussed genesis and evolution of disturbance in the form of a wave, when the flow is excited by a time-harmonic localized source. Also, in this eigenvalue formulation, there is an implicit view that the monochromatic disturbance source is placed at the wall and the created disturbances decay with height. In a noisy experimental device, there are distributed disturbance sources that are not monochromatic and the desired decay of disturbance field with height is not possible. Even when these were accounted for by placing a vibrating diaphragm at the wall as in Taylor [8], it was not successful because the frequency of vibration was too low as compared to that predicted in the theory.

In the context of the discussion above, experimental results reported in Schubauer & Skramstad [7] are extraordinary. They were the first to realise that the experimental facilities have to be made as quiet as possible and then a deterministic wall excitation would provide response in the fluid dynamical system as predicted by theoretical analysis. During the course of the research they found that the vibrating ribbon excited near the wall was the most satisfactory means of exciting TS waves. The results clearly demonstrated not only the existence of TS waves, but also helped chart out the neutral curve that matched very well for higher Reynolds number (based on displacement thickness as the length scale) with the analytical results. This was to be expected as with increasing Reynolds number the boundary layer growth becomes progressively negligible making the parallel flow approximation used in the theory more and more valid. This experiment also emphasized the link between stability analysis and receptivity of shear layer to different types of disturbance sources.

There were some work reported in the literature (as in Ashpis & Reshotko [9] and other references contained therein) that talked about the mathematical framework of receptivity analysis. It was only in Sengupta [10] and in Gaster & Sengupta [11], first set of actual results for linear receptivity of zero pressure gradient boundary layer to wall excitation were reported for the signal problem. A signal problem corresponds to the assumption that the time behaviour of the response field is as described by the time-harmonic excitation of the shear layer. Results were obtained based on parallel flow approximation that identified the TS wave as the asymptotic part of the response field i.e. the computed solution matched with TS wave away from the exciter. Apart from this asymptotic solution, the receptivity analysis also revealed a solution in the immediate neighbourhood of the exciter - called the local solution [10–12]. In Sengupta [10], solution was obtained using the Bromwich contour integral method described in Sengupta and Rao [12] and Van Der Pol and Bremmer [13]. In Gaster and Sengupta [11], solution obtained was based on the premise that the response of the boundary layer is dominated by the least stable mode - an idea in the normal mode stability analysis. Apart from being unable to explain the effects of local solution and presence of multiple modes (including the continuous spectra), the normal mode stability analysis results do not agree with experiments at lower Reynolds numbers and higher circular frequencies.

There have been some efforts made to improve agreement of theoretical results with experiments at lower Reynolds number by including the effect of weak boundary-layer growth in the stability analysis using the ansatz that the difference between the two can be bridged by introducing a simple scaling function $A(X)$, where X is a slowly varying scale that depends upon streamwise location only. This is the basis of investigations in Gaster [14] and in Saric & Nayefeh [15]. These references employed different definitions to define the non-parallel effects in terms of (a) kinetic energy integral of the disturbance flow, (b) the integrated streamwise disturbance velocity squared over the shear layer width and (c) the imaginary part of wave growth rate etc. While there were some improvements seen for the lower Reynolds number ranges, mismatches still remained to be reconciled. An attempt was made to explain these shortcomings and some interesting observations were made that is described below and is taken from Sengupta [16].

Following the ideas in Gaster [14] and Saric and Nayefeh [15], the perturbation stream function can be defined as

$$\psi(x,y,t) = \int [A(X)\Phi_0(X,y) + \epsilon\Phi_1(X,y)]e^{i(\alpha x - \omega_0 t)}d\alpha \tag{1}$$

Here, the leading term without $A(X)$ is the same that one obtains from the parallel flow approximation and the second term is the leading correction term needed to represent the non-parallel

effects, along with that represented by *A(X)*. A formal perturbation analysis reveals the governing equations for Φ_0 and Φ_1 are given by,

$$L_2(\Phi_0) = (U - \omega_0/\alpha)(\Phi_0'' - \alpha^2\Phi_0) - U'' - (\Phi^{iv}_0 - 2\alpha^2\Phi_0'' + \alpha^4\Phi_0)/(i\alpha Re) = 0 \quad (2)$$

and

$$L_2(\Phi_1) = F_0 A + F_1 \frac{dA}{dX} \quad (3)$$

where F_0 and F_1 are expressions similar to that given in Gaster [14] and Saric and Nayefeh [15] and are functions of the mean flow quantities; various terms proportional to Φ_0 and its derivatives. It was therefore pointed out in Sengupta [16] that in trying to obtain Φ_1 from Eq. (3) one would experience secular growth, as both Φ_0 and Φ_1 are governed by the same Orr-Sommerfeld operator, an essential fact overlooked in the formulations of [14,15]. In Gaster [14] and Saric and Nayefeh [15], an equation for *A(X)* was obtained from Eq (3) by using a solvability condition and the non-parallel effects were embedded from the first term of Eq (1) only. Furthermore, unlike in the stability analysis of [14,15], when the problem is posed as a receptivity problem given in Eq. (1), satisfaction of wall boundary condition would reveal that *A*(*X*) cancels out from the numerator and denominator when it is assumed that the nonparallel effects introduce mere scaling without adding or altering eigenvalues of the corresponding linear parallel flow formulation [14, 15].

Further developments on linear receptivity analysis were reported in Sengupta et al. [17–19]. In [17], the linearized receptivity problem to localized harmonic wall excitation was studied by removing the restriction of the signal problem and it revealed that any problem found spatially unstable remains so even when it is viewed in a complete spatio-temporal framework. This was further studied for spatially stable systems to explain spatio-temporal growth of wave-fronts in [18, 19], including validating a new energy based receptivity analysis. In a variation of receptivity analysis, Seifert & Tumin [20] reported experimental and theoretical results on receptivity of adverse pressure gradient shear layer to wall excitation. The experimental results were novel and theoretical results were obtained by linear stability analysis by matching the response at a fixed location. One of the major findings of this study was that the mismatch between experiment and theory widened with increase in circular frequency. This also prompts one to include both nonlinearity and non-parallelism of the equilibrium flow and one such study was reported in Fasel & Konzelmann [21] that involved studying disturbance generation and its evolution over a flat plate boundary layer via the solution of two-dimensional Navier-Stokes equation. In this numerical study, the exciter employed was a simultaneous blowing-suction strip - as shown in the schematic of Fig. 1. In the limit of vanishing width of the strip, this is equivalent to a doublet, that helped satisfy mass conservation exactly at each time step for the stream function - vorticity formulation of the problem. The authors categorically stated that *the good agreement of some of the theories with experiments is fortuitous and that the difference between experiments and theories concerning the branch I neutral location cannot be explained by non-parallel effects*. This work restricted itself in studying the nonparallel effects of a zero pressure gradient boundary layer and not much attention was paid on nonlinear effects. A similar but complimentary study was undertaken by Venkatasubbaiah and Sengupta [22] that mainly focused on receptivity and stability of mixed convection flow past a vertical plate. The stream function-vorticity formulation included the mixed convection via Boussinesq assumption and the flow was excited by a blowing-suction strip, as in [21]. In the same paper, nonlinear aspect of receptivity for zero pressure gradient shear layer without heat transfer and the associated leading spatio - temporal wave fronts are also reported.

So far our discussion on calculating receptivity of boundary layers is restricted to specific wall excitation type. Efforts have been made earlier by different investigators to study the receptivity of boundary layers to convected disturbances in the free stream. The effects of free stream turbulence on the stability of laminar boundary layers also comes under this category. Some of the most relevant experimental and theoretical studies are listed here in [23–30]. The types of disturbances studied in the experiments correspond to passing wakes and vortices [23,25,26,28,30] and free stream turbulence [24,26,27,30]. In the numerical simulations [27–30], the major issue is to decide upon the convecting speed of the disturbances in the free stream. There appears to be some misunderstanding on this issue (discussed in [27,30]) as many researchers have erroneously assumed that vortices will travel with the

free stream speed and that invariably shows the response field to be damped. However, a detailed analysis by Sengupta et al. [30] has clarified this issue via simulations and analytical results that there exists a narrow band of convection speed of disturbances (between 0.26 to 0.33 times the free stream speed) at which the receptivity is maximum for periodically passing wakes. Created response field by such excitations continues to be wave packets consists of TS waves - however, they amplify much faster than that is experienced by disturbances created by constant frequency wall exciter.

In [28,31], the authors discuss about transition that takes place in fluid flow without the appearance of TS waves and is caused by free stream turbulence. The work in [28] identifies the bypass events with the appearance of upstream propagating modes and turbulent spots created in the outer part of the shear layer. The analytical explanation for the existence of upstream propagating modes were provided earlier in [27] and other references contained therein. These type of disturbances are still within the purview of linear stability theory caused by periodic disturbance sources in the free stream. Another bypass mode was shown theoretically and experimentally in [32,33] that is created by convecting a periodic disturbances in the free stream. In many practical situations, actual transition will be a consequence of the presence of some or all the prototypical mechanisms discussed so far.

In the present work, we focus upon the nonlinear receptivity of a zero pressure gradient boundary layer excited by a blowing-suction type of wall-exciter [21,22]. The main intention is to show the role of multi-modal nature of the instability of the flow field, that cannot be explained by normal mode analysis practised in the linear stability theory. The multi-modal interactions cause disturbance growth in regions of flow, which otherwise have been pronounced as stable by linear spatial stability analysis. Such multi-modal interactions have also been attempted to be explained as weakly nonparallel effects [14,15]. In the next section the governing equations and the used numerical methods have been described. In section 3, numerical results have been presented along with their detailed discussion. Section 4 contains the summary and closing remarks on the present work.

3. GOVERNING EQUATIONS AND NUMERICAL METHOD

The two-dimensional Navier-stokes equations in stream function-vorticity formulation are solved here and are given below in non-dimensional form with respect to reference length, velocity, time, vorticity and stream-function respectively as L, U_∞, $\frac{L}{U_\infty}$, $\frac{U_\infty}{L}$, LU_∞,

$$\frac{\partial \omega}{\partial t} + \vec{V} \cdot \nabla \omega = \frac{1}{Re} \nabla^2 \omega \tag{4}$$

$$\nabla^2 \psi = -\omega \tag{5}$$

Here the Reynolds number Re is defined as $Re = \frac{LU_\infty}{\nu}$, where ν is the kinematic viscosity. The out of plane vorticity is given by ω and the velocity is related to the stream function by $\vec{V} = \nabla \times \Psi$, where $\Psi = (0, 0, \psi)$. The $(\psi - \omega)$ formulation is preferred here due to its accuracy and efficiency in satisfying mass conservation exactly everywhere. The flow is computed in the transformed orthogonal $(\xi - \eta)$ plane that is utilized for grid refinement whenever necessary. In a transformed orthogonal $(\xi - \eta)$ plane, the vorticity-transport equation and the stream-function equation transforms to,

$$\frac{\partial \omega}{\partial t} + \frac{\partial \psi}{\partial \eta}\frac{\partial \omega}{\partial \xi} - \frac{\partial \psi}{\partial \xi}\frac{\partial \omega}{\partial \eta} = \frac{1}{Re}\frac{1}{h_1 h_2}\left[\frac{\partial}{\partial \xi}\left(\frac{h_2}{h_1}\frac{\partial \omega}{\partial \xi}\right) + \frac{\partial}{\partial \eta}\left(\frac{h_1}{h_2}\frac{\partial \omega}{\partial \eta}\right)\right] \tag{6}$$

$$\frac{\partial}{\partial \xi}\left(\frac{h_2}{h_1}\frac{\partial \psi}{\partial \xi}\right) + \frac{\partial}{\partial \eta}\left(\frac{h_1}{h_2}\frac{\partial \psi}{\partial \eta}\right) = -h_1 h_2 \omega \tag{7}$$

where the contra-variant components of the velocity vector are given by

$$u = \frac{1}{h_2}\frac{\partial \psi}{\partial \eta} \tag{8}$$

$$v = -\frac{1}{h_1}\frac{\partial \psi}{\partial \xi} \tag{9}$$

Where h_1 and h_2 are the scale factors of the transformation given by, $h_1 = (x_\xi^2 + y_\xi^2)^{1/2}$ and $h_2 = (x_\eta^2 + y_\eta^2)^{1/2}$. In the used transformed grid, ξ is in the direction parallel to the wall and η is in the wall-normal direction. Hence the transformation is given by $x = x(\xi)$ and $y = y(\eta)$, so that $h_1 = x_\xi$ and $h_2 = y_\eta$. The equations (6) and (7) are known as the vorticity transport equation (VTE) and stream function equation (SFE), respectively.

3.1. Boundary and initial condition

Specification of proper boundary conditions and their implementation in the numerical method is an issue of great importance in DNS. To obtain higher resolution and easily implement boundary conditions, we compute the equations in the orthogonally transformed ($\xi - \eta$) plane, obtained from the Cartesian frame via the transformation given by,

$$x(\xi) = x_{\text{in}} + L_D[1 - \frac{tanh(\beta(1-\xi))}{tanh\beta}] \tag{10}$$

$$y(\eta) = L_h[1 - \frac{tanh(\beta(1-\eta))}{tanh\beta}] \tag{11}$$

with $0 \leq \xi, \eta \leq 1$. In the above, x_{in} is the streamwise coordinate of the inflow of the computational domain whose streamwise extent is given by $L_D = x_{\text{out}} - x_{\text{in}}$, where x_{out} is the location of the outflow of the computational domain taken as $10L$. Similarly, the second transformation relates the wall-normal physical distance of L_h (equal to L), to the transformed co-ordinate η. Here, we have taken $\beta = 2.0$ to obtain grid clustering near the inflow and the wall. A very localised wall-excitation is applied at a location near the inflow and for this reason the grid clustering in the vicinity is required. This type of tangent-hyperbolic transformation apart from producing desired grid clustering, also helps in reducing aliasing error and is widely used in simulations [34].

In this computation, the steady-state solution is obtained first and thereafter we perturb the flow by providing excitation at the wall. In the following, we discuss the boundary conditions separately - so that the process of obtaining the mean and disturbed flows are clearly revealed. For the disturbance flow, these boundary-conditions reveal the nature of applied excitation at the wall. However, the boundary condition for equations (6) and (7) will be used for the total quantities (without splitting them into mean and disturbance components) for the receptivity calculations.

In computing the steady-flow, following wall-boundary conditions have been used,

$$\psi_{\text{wall}} = const. \qquad \omega_{\text{wall}} = -\frac{1}{h_2^2}\frac{\partial^2 \psi}{\partial \eta^2}\,|\,wall \tag{12}$$

For the computation of the perturbed flow with excitation at the wall, the boundary conditions used are

$$v_{\text{wall}} = (-\frac{1}{h_1}\frac{\partial \psi}{\partial \xi})|_{\text{wall}} \qquad \omega_{\text{wall}} = -\frac{1}{h_1 h_2}\frac{\partial}{\partial \xi}(\frac{h_2}{h_1}\frac{\partial \psi}{\partial \xi}) - \frac{1}{h_2^2}\frac{\partial^2 \psi}{\partial \eta^2}\,|_{wall} \tag{13}$$

The boundary condition for the stream function at the wall has been deduced from the zero normal velocity for the equilibrium flow and from the prescribed time-dependent normal velocity at the wall, for the perturbed flow. The wall vorticity has been calculated imposing no-slip condition at the wall in the expression for SFE. For the receptivity calculation, the prescribed time-dependent normal velocity at the wall corresponds to a simultaneous blowing and suction on a localised strip (as in [21,22]). The prescribed time-dependent normal velocity at the wall is given by:

$$v_{\text{wall}}(x) = \begin{cases} A_m(x) sin(\beta_d t) & \text{for } x_1 \le x \le x_2 \\ 0 & \text{for } x \le x_1 \text{ or } x \ge x_2 \end{cases} \tag{14}$$

where β_d is the non-dimensional disturbance angular velocity and $A_m(x)$ is the amplitude of the imposed disturbance. Here x_1 and x_2 represent the beginning and the end of the streamwise extent of the strip along the wall. The amplitude function is defined along the blowing-suction strip (as given in Fasel and Konzelmann [21]) by:

$$A_{FK}(x) = 15.1875\left(\frac{x - x_1}{x_{st} - x_1}\right)^5 - 35.4375\left(\frac{x - x_1}{x_{st} - x_1}\right)^4 + 20.25\left(\frac{x - x_1}{x_{st} - x_1}\right)^3 \tag{15}$$

for $x_1 \le x \le x_{st}$ and

$$A_{FK}(x) = -15.1875\left(\frac{x_2 - x}{x_2 - x_{st}}\right)^5 + 35.4375\left(\frac{x_2 - x}{x_2 - x_{st}}\right)^4 - 20.25\left(\frac{x_2 - x}{x_2 - x_{st}}\right)^3 \tag{16}$$

for $x_{st} \le x \le x_2$where $x_{st} = \frac{x_1 + x_2}{2}$, where we have taken $A_m = \alpha A_{FK}$.

At the inflow and at the far-field boundary (at the top of the domain), to calculate steady as well as the perturbed flow the following boundary conditions have been used,

$$U_\infty = 1 \qquad \omega = 0 \tag{17}$$

At the outflow, following convective boundary condition on vorticity has been used,

$$\frac{\partial \omega}{\partial t} + U_c \frac{\partial \omega}{\partial t} = 0 \tag{18}$$

The value of the convective speed U_c has been chosen as $0.5U_\infty$. The stream-function ψ, at the outflow boundary has been calculated from the condition $\frac{\partial v}{\partial x} = 0$ which using (9) translates in terms of ψ as

$$\frac{\partial}{\partial \xi}\left(\frac{1}{h_1}\frac{\partial \psi}{\partial \xi}\right) = 0 \tag{19}$$

3.2. Numerical discretization

In the computations, the terms $\frac{\partial \omega}{\partial \xi}$ and $\frac{\partial \omega}{\partial \eta}$ representing convection in the VTE are discretised using high resolution OUCS3 compact schemes developed in Sengupta *et al*. [34,35]. The terms $\frac{\partial \psi}{\partial \xi}$ and $\frac{\partial \psi}{\partial \eta}$ appearing in the VTE are discretized using second order central difference scheme. This is done to minimize errors caused by aliasing. Since the VTE specifically tells us about the transport of vorticity, and since the vortices are like wave-packets we need to resolve the vortices as accurately as possible maintaining their correct group velocities as they convect. However, the convection terms are non-linear and hence if we use high resolution schemes to discretize them then that would lead to aliasing error. The diffusion term that appears in the VTE as well as the terms involving Laplacian operator that appears in the SFE are all discretised using second order central difference scheme. The compact OUCS3 scheme [34,35] used here to calculate first derivative terms are represented by primes on the left hand side of the following equations. To begin with, explicit equations are used for the near-boundary points given by,

$$u_1' = \frac{1}{h}(-3u_1 + 4u_2 - u_3)$$

$$u_2' = \frac{1}{h}\left[\left(\frac{2\beta_1}{3} - \frac{1}{3}\right)u_1 - \left(\frac{8\beta_1}{3} - \frac{1}{2}\right)u_2 + (4\beta_1 + 1)u_3 - \left(\frac{8\beta_1}{3} + \frac{1}{6}\right)u_5 + \frac{2\beta_1}{3}u_5\right]$$

with β_1, a floating constant used to stabilize computations and improving dispersion relation preservation of the overall numerical scheme. If there are N points in that direction, for the interior points ($3 \le j \le N-2$), following implicit equations are used in the scheme [34,35],

$$p_{j-1}u'_{j-1} + u'_j + p_{j+1}u'_{j+1} = \frac{1}{h}\sum_{k=-2}^{k=2} q_k u_{j+k}$$

where $p_{j\pm1} = D \pm \frac{\eta}{60}$; $q \pm 2 = \pm\frac{F}{4} + \frac{\eta}{300}$; $q \pm 1 = \pm\frac{E}{2} + \frac{\eta}{30}$; $q_0 = -\frac{11\eta}{150}$

with $D = 0.3793894912$; $E = 1.57557379$; $F = 0.183205192$ and $\eta = -2.0$. The stencil for $j = N-1$ and $j = N$ are similar to the stencil written for $j = 2$ and $j = 1$, respectively. For better numerical properties, one requires to use $\beta = -0.025$ for $j = 2$ and $\beta = 0.09$ for $j = N-1$. The VTE is time advanced using the 4th order Runge-kutta scheme with time-step of $\Delta t = 5.0 \times 10^{-5}$. The discretized SFE is solved using unpreconditioned Bi-CGSTAB algorithm [36].

4. RESULTS AND DISCUSSION

To calculate the receptivity of a zero pressure gradient boundary layer, Navier-Stokes equation given in the previous section has been solved with the following numerical parameters. We have chosen the length scale such that *Re* based on the reference length scale L is 10^5. The computational domain along the streamwise direction domain is taken as $-0.05 \le x \le 10$; while in the wall-normal direction, the computational domain is taken as $0 \le y \le 1$. A total of 1600 points in the streamwise and 600 points in the wall-normal directions are taken. For this shear layer, the reference length is taken as $L \cong 60 \times \delta^*_D$, where δ^*_D is the displacement thickness at the outflow of the computational domain shown in Fig. 1(a). We have taken the grid mapping in such a way that the wall-resolution is given by: $\Delta y_0 = 2.455 \times 10^{-4}$ and the smallest grid size in the streamwise direction is given by: $\Delta x_0 = 9.218 \times 10^{-4}$. Simulation results are presented here for the case when the suction-blowing strip exciter is located between $x_1 = 0.22$ and $x_2 = 0.264$ that is excited harmonically at a circular frequency of β_d. Different values of the amplitude of the excitation is calculated with $A_m = \alpha A_{FK}$, where A_{FK} is the amplitude function taken in Fasel and Konzelmann [21], as given here in Eqs. (15) and (16). Here, the results are shown for only $\alpha = 0.01$

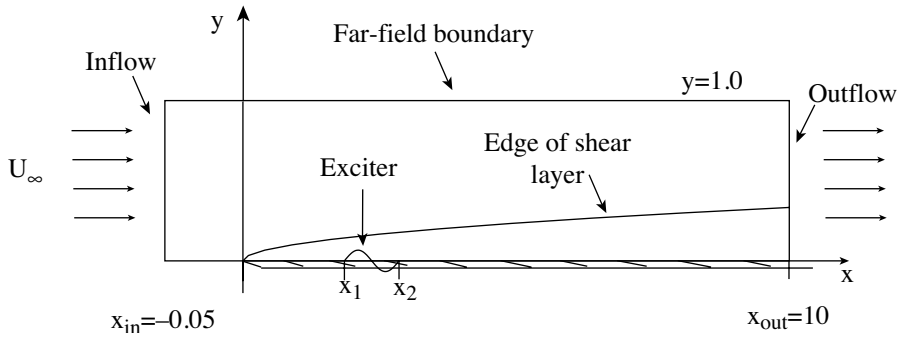

Fig. 1(a) Schematic of the flow and the computational domain including the simultaneous blowing and suction (SBS) strip.

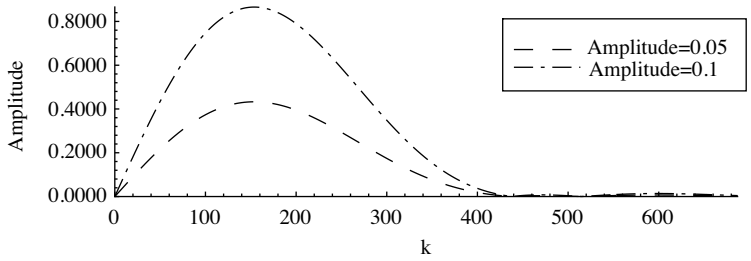

Fig. 1(b) Fourier transform of the input disturbance through the SBS strip for the amplitudes of excitation $0.05A_{FK}$ and $0.1A_{FK}$ with A_{FK} as defined in equations (15) and (16). The exciter is located from $x_1 = 0.22$ to $x_2 = 0.264$.

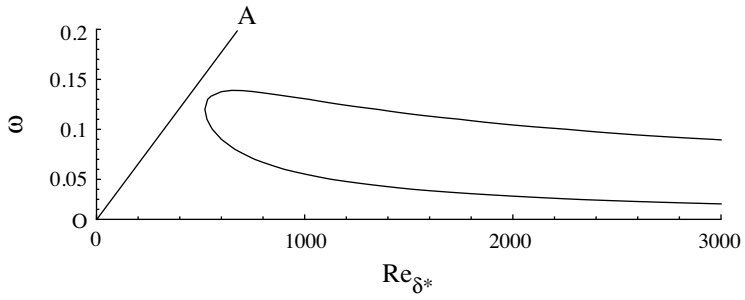

Fig. 1(c) The neutral curve based on linear stability theory. The straight line OA corrosponds to the constant non-dimensional frequency parameter 3.0×10^{-4} considered here for simulations.

and 0.05, while the input spectrum shown in Fig. 1(b) compares the cases of $\alpha = 0.05$ and 0.10. This comparison shows that various wave numbers in the input do not necessarily scale by the maximum amplitude of the various cases studied. This type of nonlinear attribute of input was also studied and reported in [22] for the zero pressure gradient boundary layer and will not be repeated here.

The non-dimensional frequency parameter that is often used to present stability analysis results relates the circular frequency with the Reynolds numbers by $F_f = \beta_d/Re$- as in [22]. In the present investigation, we have chosen specifically the value of F_f equal to 3.0×10^{-4}. The reason for this choice of frequency will be apparent by looking at the neutral curve shown in Fig. 1(c) that is obtained using a parallel flow stability analysis. Any disturbance that is created by a constant frequency wall exciter follows a ray starting from the origin - as shown in this figure for the chosen frequency indicated by OA. As the flow is linearly stable for all rays that remain outside the neutral loop, the chosen frequency represents a linearly stable case. Upon performing receptivity calculations by solving the full Navier-Stokes equation, if we perceive any qualitative differences from linear stability results, then that could be due to either nonparallel or nonlinear or due to both the effects. This is the central theme of the present work.

To study the receptivity of a boundary layer, it is necessary to first obtain an equilibrium state whose response to well-defined disturbances have to be investigated. For this purpose, the VTE and SFE given by Eqs. (6) and (7) are solved in succession till such a time when the flow evolves to the equilibrium state. For the present investigation, this is continued till $t = 30$ to obtain the equilibrium flow. In reporting the receptivity of this steady state, we apply the simultaneous blowing-suction excitation at the wall given by Eqs. (14)-(16) and such results are shown in Fig. 2 for the case of $F_f = 3 \times 10^{-04}$ and $A_m = 0.05\ A_{FK}$. In showing the signal in Fig. 2(a), the origin refers to the leading edge of the flat plate. From the solution of Eqs. (6) and (7), one obtains instantaneous values of vorticity and velocity components. The disturbance quantities are obtained (as displayed in Fig. 2) by subtracting the mean from the total quantity. As noted earlier, this corresponds to a spatially stable case in linear theory. For the displayed data at all heights, the disturbance velocity has a local component in the immediate neighbourhood of the exciter (will be referred henceforth as the local solution) and this is followed by the asymptotic wavy solution - earlier identified as the TS wave. However, one must distinguish between the TS wave obtained by the normal mode analysis and the asymptotic solution reported here. In normal mode analysis, only the least stable eigenmode is tracked and reported, ignoring the existence and the contribution of other modes. In contrast, the present approach produces solution that is contributed by all the discrete and continuous modes.

The displayed variation of streamwise disturbance velocity with streamwise coordinate at different heights over the plate indicate an interesting phenomenon. This solution corresponds to the time $t = 20$. While the linear normal mode analysis, predicts this flow field to be stable, we notice that barring the top and bottommost frames in Fig. 2(a), the disturbances actually grow spatially at intermediate heights. All the frames clearly indicate the presence of multiple modes and that is also directly evident from the multiple peaks of the Fourier transform of these signals shown in Fig. 2(b). The Fourier amplitudes show the dominant normal mode near the wall, while multiple dominant modes are seen in the third and fourth frames showing the transform. Also, one notices the contribution responsible for the local solution as the distant low peak at high wave numbers in Fig. 2(b). It is easy to identify the peaks in

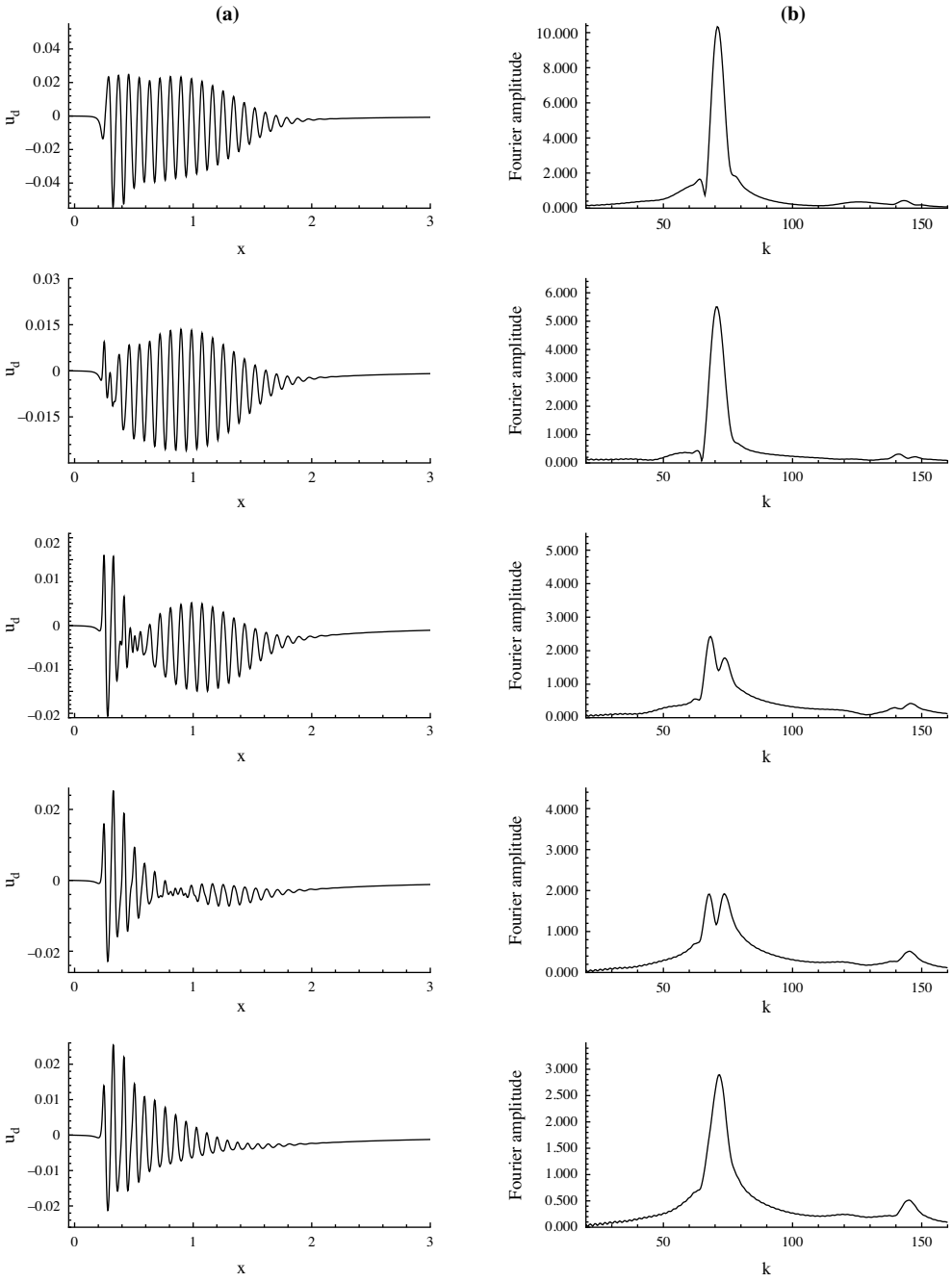

Fig. 2(a) u_d plotted as a function of x for t=20 at the heights 0.00385; 0.00521; 0.00662; 0.00808; 0.00958 and 0.0144 respectively from top to bottom. The signals are for the SBS strip excitation amplitude of $A_m=0.05A_{FK}$; $F_f=3.0\times10^{-4}$ and exciter location between x_1 = 0.22 and x_2 =0.264. (b) Fourier transforms of the signals shown in (a).

the spectral plane with the solution in the physical plane through Abel's and Tauber's theorem [13]. The second to fourth frames in Fig. 2(a) clearly show different streamwise stretches at different heights over which the disturbance actually grows with *x* corresponding to a particular mode that moves downstream at a faster speed. The presence of this mode becomes weaker as the height increases. However, there is another damped mode that dominates with increasing height over the plate. It is noted that in earlier nonparallel studies (as referred to in [21]), various investigators have tried to explain experimental data that indicated instability at particular heights for the streamwise disturbance velocity components.

It has been variously noted in [12, 17–19] that there are no particular physical reasons as to why one has to adopt either spatial or temporal framework in studying boundary layer stability. This is also readily apparent from the information in Figs. 2 and 3. An interesting aspect of the computed results is noted with respect to time variation - as shown in Fig. 3(a) for signals collected at a distance of $x = 0.3L$ from the leading edge at the indicated heights. Despite the fact that the fluid dynamic system is excited at a single constant frequency (β_d), the Fourier transform in Fig. 3(b) indicates presence of superharmonics at all heights and of different proportions. From Fig. 1(c) one clearly notes the corresponding normal modes to

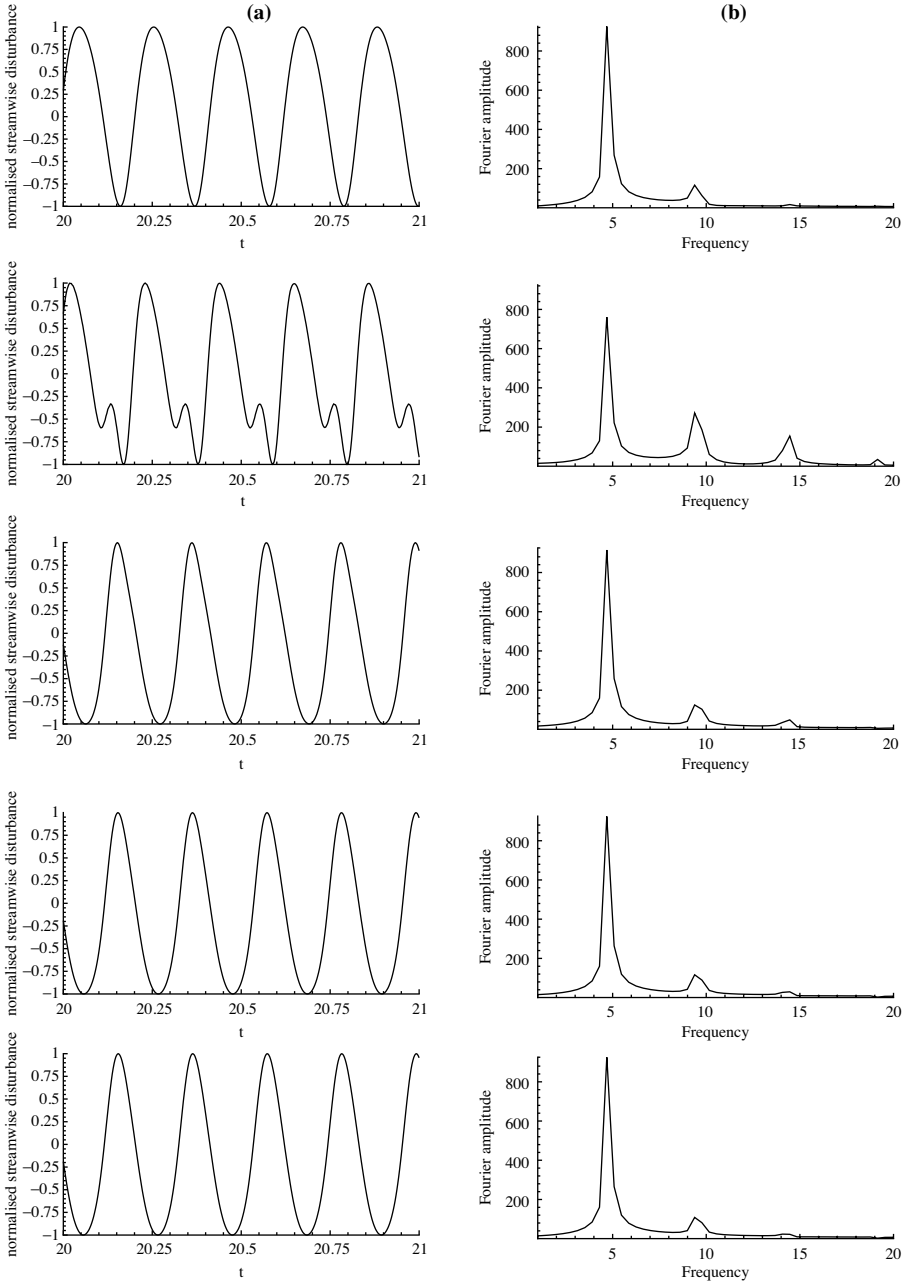

Fig. 3 (a) Normalised streamwise disturbance velocity time series plotted for a distance of 0.3 from the exciter at the heights 0.00385; 0.00662; 0.00808; 0.00958 and 0.0144, respectively from top to bottom. The figure is shown for the SBS strip excitation amplitude of $0.05A_{FK}$, $F_f=3.0\times10^{-4}$ and the exciter location between $x_1 = 0.22$ and $x_2 = 0.264$. (b) Fourier transforms of the signal shown in (a) clearly show the presence of superharmonics.

be more stable from linear stability point of view for these additional superharmonics. Of specific interest is the data for $y = 0.00662$ and 0.00808 that shows the presence of strong second and third harmonics. In Fig. 2(a) also, we noted most pronounced instability at these heights. Thus, the disturbance growth at these heights must be related to nonlinear effect and is experienced at intermediate heights only.

Apart from the fact that the instability is noted at intermediate heights, we also note the similarity of flow field at heights very close to the wall and those in the outer edge of the boundary layer. This aspect is depicted in Fig. 4(a), where spatial variation of the streamwise disturbance velocity is shown for

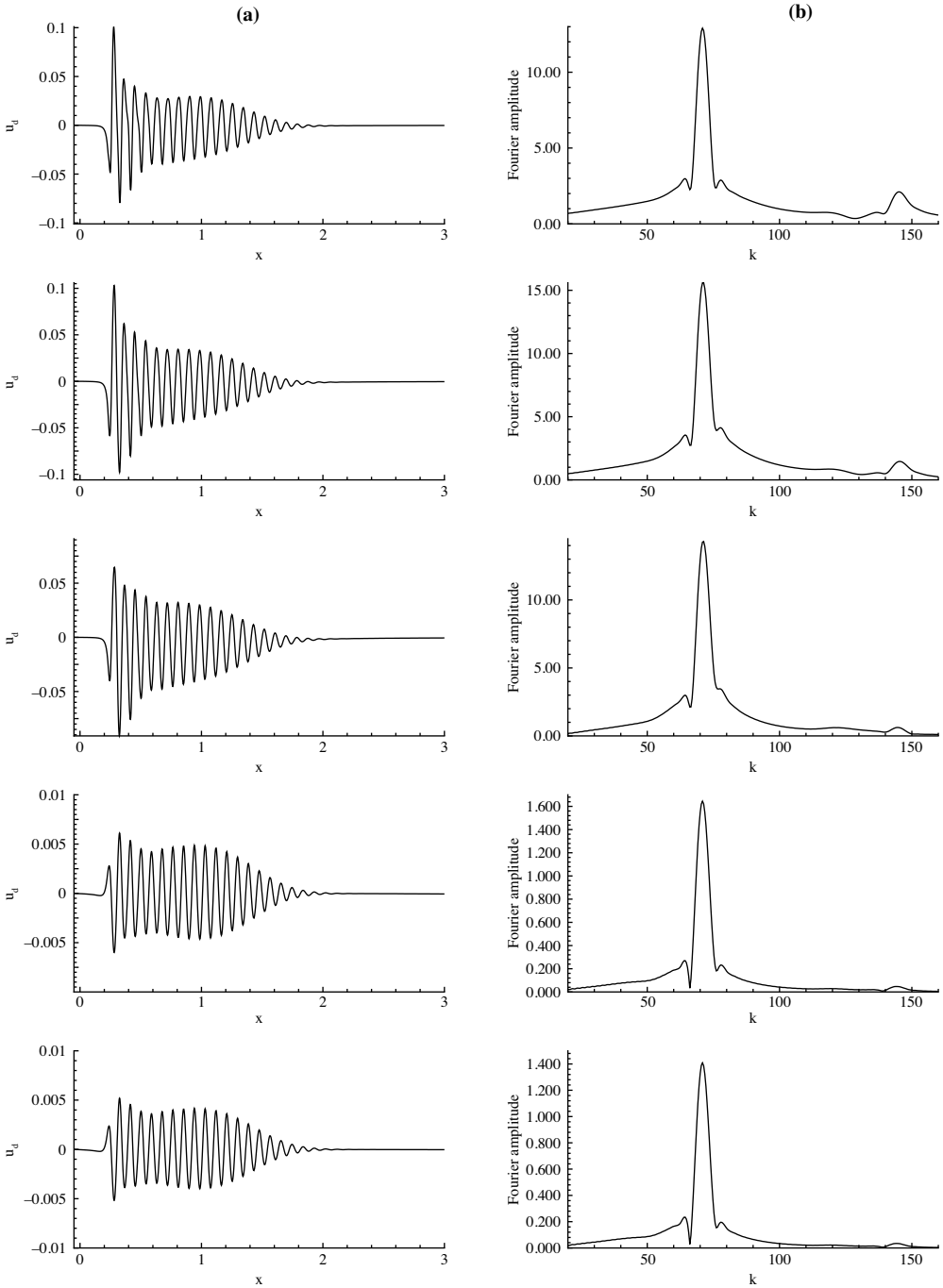

Fig. 4 (a) Streamwise disturbance velocity plotted against x for t=20 for the SBS strip excitation with A =0.05A_{FK}, F_f=3.0×10^{-4} and exciter located between x_1 = 0.22 and x_2 = 0.264. The data are shown for the heights 0.00124; 0.00252; 0.00384; 0.03 and 0.032, respectively from top to bottom. (b) Fourier transform of the signals shown in (a).

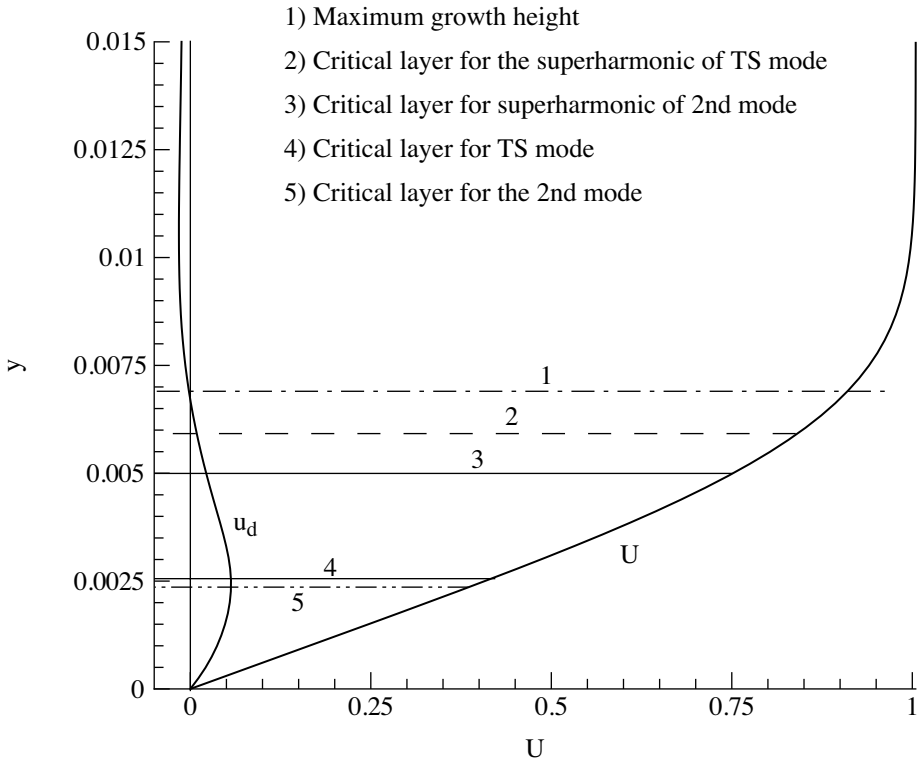

Fig. 5 Mean and disturbance component of streamwise velocity shown along with various estimates of critical layer for the TS and the second spatial mode. The line-1 indicates the height where maximum local spatial growth is noted. Presented data are for the SBS excitation with A_m=0.05A_{FK}; F_f=3.0×10^{-4} and the exciter located between x_1 = 0.22 and x_2 = 0.264.

points those are either very near the wall or are in the outer part of the shear layer. Corresponding Fourier transform of these signals are shown in Fig. 4(b). At these heights, signals display a range of x for which they remain neutral, while in the other part, the signals decay with streamwise distance. Thus, the Figs. 2 to 4 show that this particular case represents nonlinear receptivity at intermediate heights; neutral stability near the wall and in the outer part of the boundary layer.

Presence of growing solution at intermediate heights is further investigated by plotting the mean and disturbance component of streamwise velocity with height, in Fig. 5. In the same figure, we have identified the height at which the direct simulation indicates maximum growth rate by drawing the horizontal line-1. We have already noted that there are multiple spatial modes (including the normal mode, identified as the TS mode in the figure) and superharmonics of the excitation frequency present in the simulated cases. Their effects are different at different heights, as shown already in Figs. 2 to 4. For example, in Fig. 3, one can clearly note the presence of dominant superharmonics at y = 0.00662 and 0.00808. While they are also noted at different heights, they play secondary roles there. In discussing this aspect of Fig. 3, we have reasoned that these are essentially nonlinear effects which come into play in the proximity of critical layers. These critical layers for the TS and the second modes are identified in Fig. 5 - their location indicated by lines 2 to 5. It is seen that the maximum growth height is located closer to the critical heights of the TS and second modes corresponding to the first superharmonics-at which the linearized convection terms disappear in the governing Orr-Sommerfeld equation for the TS mode-fundamental frequency combination.

4.1. Role of amplitude of excitation

To understand the role of the amplitude of excitation through the blowing-suction strip, another case is computed with identical excitation parameters, except the amplitude of wall excitation is doubled to A_m = 0.10 A_{FK}. We note that the used numerical methods used here do not attenuate the signal

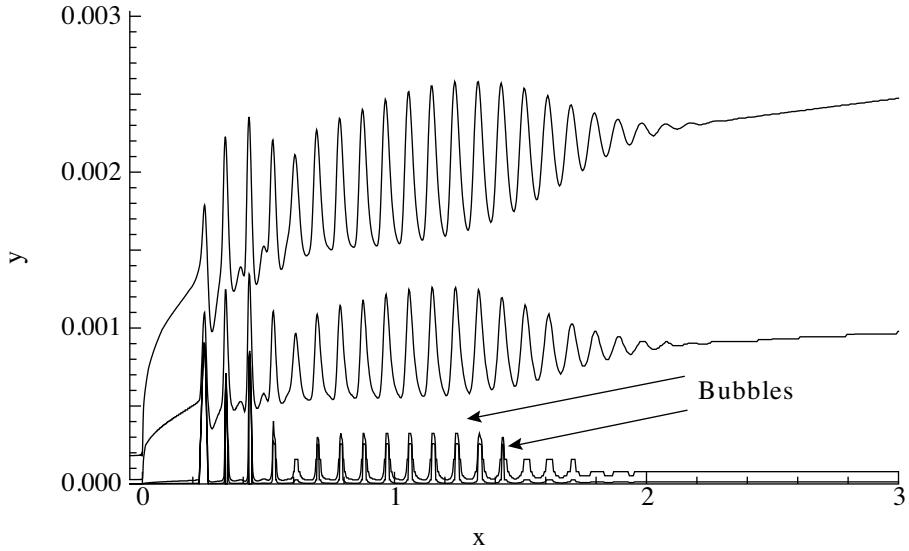

Fig. 6 Streamline contours shown in the physical plane for t=20 for the case of $A_m=0.10A_{FK}$; $F_f=3.0\times10^{-4}$ and exciter located between $x_1 = 0.22$ and $x_2 = 0.264$. Note the micro-bubbles near the exciter on the plate.

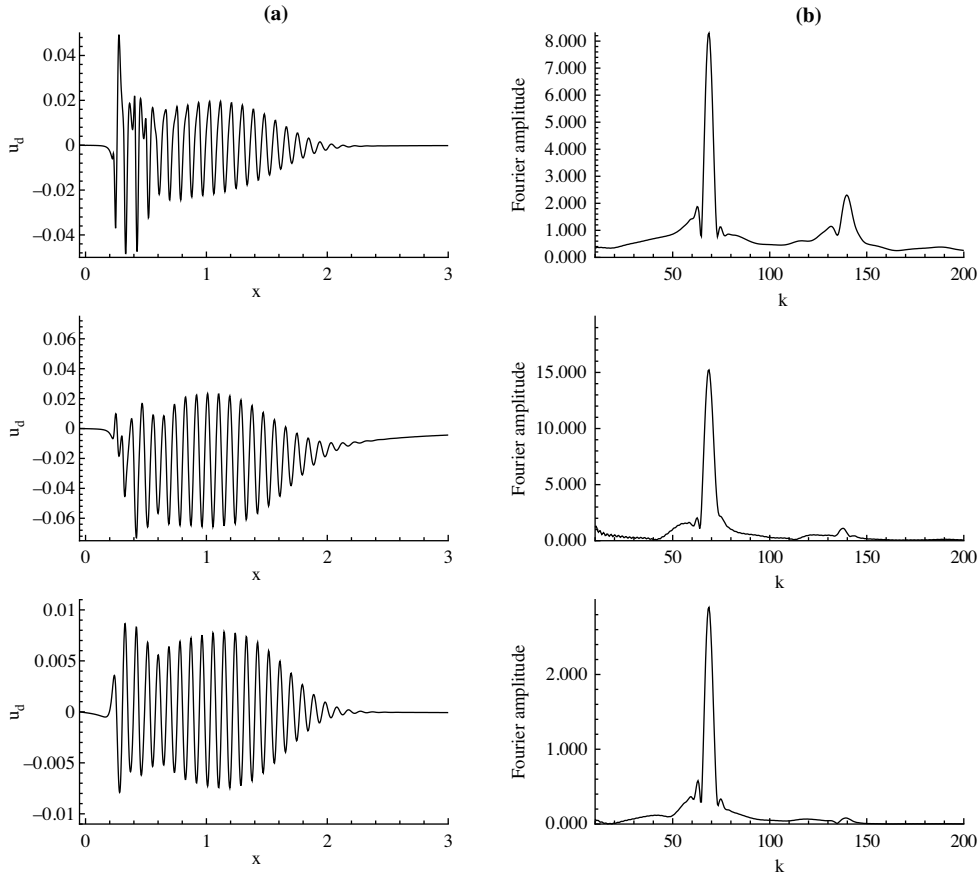

Fig. 7(a) Disturbance streamwise velocity component plotted for the heights 0.00245; 0.00521 and 0.035, respectively from top to bottom at t=20. Results presented are for the SBS strip excitation with $A_m=0.10A_{FK}$; $F_f=3.0\times10^{-4}$ and the exciter located between $x_1 = 0.22$ and $x_2 = 0.264$. (b) Fourier transform of the signals shown in (a).

artificially and it is for this reason that the amplitudes considered here are a small fraction of the excitation amplitude taken in [21]. Even the large amplitude case considered in this subsection corresponds to the amplitude that is one-tenth the amplitude considered in [21]. Doubling of the blowing-suction amplitude causes micro-separation near the exciter, on the plate. Resultant steady separation bubbles are confined to small height at the wall - as shown in the stream function contours shown in Fig. 6 at t = 20. Only a few representative contours have been shown plotted in this figure that clearly show the micro-bubbles near the exciter seen up to $x \leq 1.6$ only. However, effects of the present bubbles are noted in the other contours shown at other heights.

To understand the dynamics of this case better, instantaneous snapshot at $t = 20$ is shown for the streamwise disturbance velocity variation with x at three heights in Fig. 7(a). In the figure on the right hand side, corresponding Fourier transform is shown alongside in Fig. 7(b) that helps identify various components of the solution in the physical space. There is an effect of increasing the amplitude of excitation that is noted here for the increased amplitude. Presence of separation bubbles causes the fluid particles outside the bubbles to traverse in the transverse direction more than in the streamwise direction and this is reflected in the lower value of u_{d} for the higher A_m case, as can be ascertained by comparing Figs. 7 with 2 and 4. Also, these micro-bubbles interfere with the local solution that is clearly seen in the Fourier transform of Fig. 7(b) as compared to that shown in Fig. 2(b) for the peak corresponding to the local solution near $k = 145$. In fact, for the data shown at the second height next to the wall ($y = 0.000245$), the local solution peak is more pronounced as compared to the local solution peaks for $y = 0.00521$ and $y = 0.035$. We conjecture that with increasing the width of the exciter and increasing the amplitude of excitation further, separation bubbles will be more pronounced, that could interfere destructively with the TS waves - as has happened in this case in a low intensity. However,

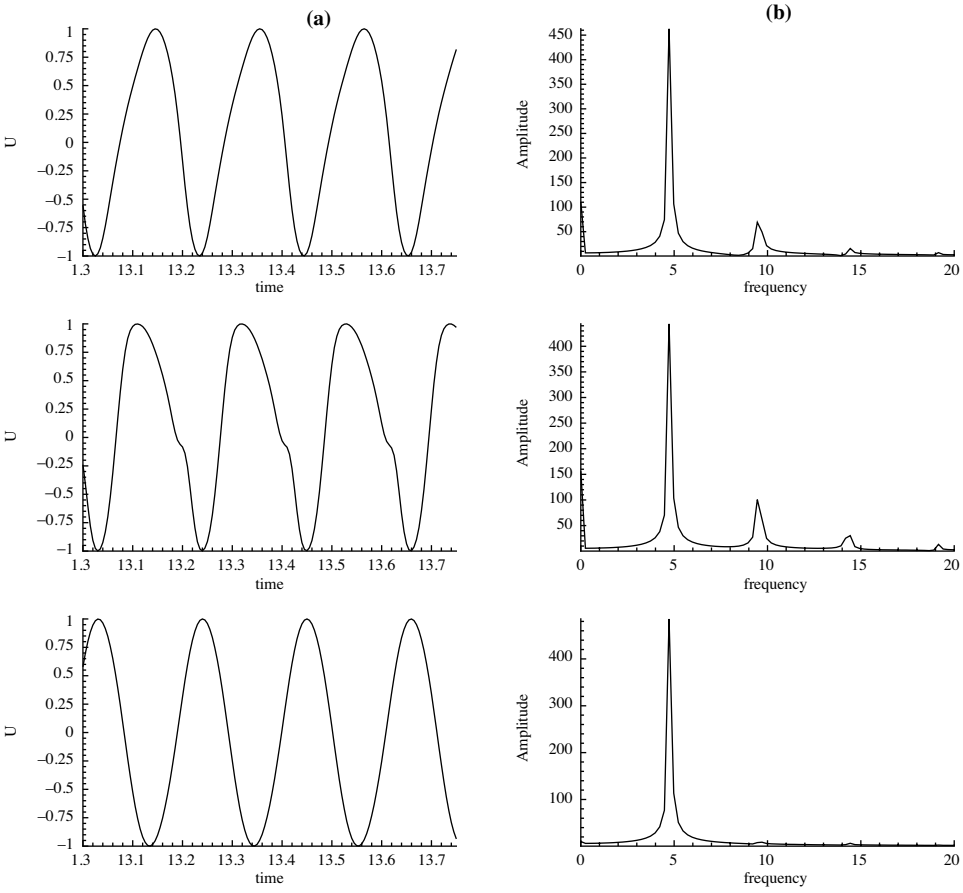

Fig. 8 (a) Normalised streamwise disturbance velocity time series plotted at a distance of 0.3 away from the exciter, at the heights: 0.00124; 0.00662 and 0.034 for the SBS strip-excitation with A_m=0.10A_{FK}, F_f=3.0×10^{-4} and the exciter located between x = 0.22 and 0.264. (b) Fourier transform of the signal shown in (a).

presence of TS waves is unmistakable for this case of $A_m = 0.1\ A_{FK}$. There is another difference for the results of the present case that is noted in the outer part of the boundary layer. For $A_m = 0.05A_{FK}$ case, solution shown at $y = 0.032$ in Fig. 4 did not show any instability. In contrast, for the case of $A_m = 0.10\ A_{FK}$ the results shown for $y = 0.035$, one can distinctly see the presence of a streamwise stretch over which the disturbance actually grows.

In Fig. 8(a), the time series for the streamwise disturbance velocity is shown at $x = 0.3$ for the three indicated heights. These time series' are multi-periodic, as it is evident from the Fourier transform shown in Fig. 8(b). Once again, the dominant presence of second and third harmonics are noticeable in the interior of the shear layer (at around $y = 0.00662$), similar to the case shown in Fig. 3. The superharmonics are not seen for $y = 0.034$ and above in this case.

Thus, the results shown so far indicate why the experimental observation of nonparallel and nonlinear effects were not predicted satisfactorily using weakly nonlinear and nonparallel theories. While we have only presented results showing the effects of increasing the amplitude of excitation, more simulations have been planned to further investigate the roles of frequency of excitation, width and location of the SBS strip in near future.

5. SUMMARY

We have reported the receptivity of zero pressure gradient boundary layer to time-harmonic wall excitations of different amplitudes here. While the effects of different frequencies and width of the exciter strip is planned for future, we have reported here a single frequency case for two different amplitudes to highlight the nonlinear and boundary layer growth effects.

Highly accurate numerical methods used here are not unduly dissipative and dispersive that allows one to investigate systematically the above mentioned effects by solving the Navier-Stokes equation for the receptivity study. In the present investigation, we have used amplitudes of excitations those are only 5% and 10% of the amplitudes considered in Fasel and Konzelmann [21]. We have investigated a specific frequency that is known to produce stable normal mode obtained by linear spatial instability analysis method. However, the corresponding earlier experiments in [7] and those referred in [14,15] have reported them to be selectively unstable. Various authors have attributed this anomaly to the growth of the boundary layer and the neglected nonlinearity in the normal mode analysis. Presented results here tries to reconcile the same via direct simulation of Navier-Stokes equation. In this approach most of the assumptions of linear theory can be removed (excepting the fact that the flow is two-dimensional) and one can mainly account for all the present modes in a spatio-temporal framework. In consonance with the results of Bromwich contour integral method as applied to this problem in [12,17–19] for the linear receptivity approach, we have identified the numerical response as a combination of local and asymptotic solution.

For the lower amplitude case, we have identified the local and asymptotic solution contributed by different modes and their interactions. Resultant solution indicate instability at some intermediate heights that seems compatible with the experimental observations. This is attributed to neglected nonlinearity that appears to be important at the critical height corresponding to the spatial modes due to the first superharmonics of the excitation frequency.

When the amplitude of excitation is doubled, while keeping other parameters of the simultaneous blowing-suction strip the same, we notice clearly the amplitude effects in terms of some micro-bubbles forming on the plate, near the exciter. These have the effects of reducing the streamwise distrubance velocity magnitude, while creating high wave number disturbances affecting the local solution. However, the wave number of the asymptotic solution do not change with the doubling of the excitation amplitude.

REFERENCES

1. Heisenberg, W. Über stabilität und turbulenz von flüssigkeitsströmen. Ann. Phys. Lpz. (4), **74**, 577–627, 1924. (Translated as 'On stability and turbulence of fluid flows'. Tech. Memo. NACA, Wash. No. 1291, 1951)
2. Tollmien, W. The production of turbulence. NACA TM-609, 1931.
3. Schlichting H. Zur ensteheung der turbulenz bei der plattenströmung. Nachr. Ges. Wiss. Göttingen, Maths-Phys. Klasse no. 181–208, 1933.
4. Kelvin, Lord Hydrokinetic solutions and observations. Phil. Mag. (4) 42, 362–377, 1871.

5. Rayleigh, Lord On the stability or instability of certain fluid motions. In Scientific Papers. 1, 361–371, 1880.
6. Rayleigh, Lord On the stability or instability of certain fluid motions. In Scientific Papers. 3, 17–23, 1887.
7. Schubauer G.B. and Skramstad H.K. Laminar boundary layer oscillations and the stability of laminar flow. J. Aero. Sci., 14, 69–78, 1947.
8. Taylor G.I. Some recent developments in the study of turbulence. In Proc. Fifth Int. Cong. Appl. Mech. (Eds. Den Hartog J.P. and Peters H.) 1939.
9. Ashpis D.E. and Reshotko E. Vibrating problem revisited. J. Fluid Mech., 213, 531–547, 1990.
10. Sengupta, T.K. Impulse response of laminar boundary layer and receptivity. In Proc. 7th Int. Conf. Num. Meth. Laminar & Turbulent Flows. Ed. C. Taylor, 1991
11. Gaster M. and Sengupta T.K. The generation of disturbance in a boundary layer by wall perturbation: The vibrating ribbon revisited once more. In Instabilities and Turbulence in Engineering Flows (Eds. D.E. Ashpis, T.B. Gatski and R. Hirsch) Kluwer Publisher, 1993.
12. Sengupta T.K. and Rao A.K. Spatio-temporal receptivity of boundary-layers by Bromwich contour integral method. In Proc. Int. Conf. on Boundary and Interior Layers (BAIL 2006) (Eds. Lube G. and Rapin G.), Goettingen, Germany, 2006.
13. Van Der Pol B. and Bremmer H. Operational Calculus Based on Two-Sided Laplace Integral. Cambridge Univ. Press, U.K., 1959.
14. Gaster M. On the effects of boundary-layer growth on flow stablity. J. Fluid Mech., 66(3), 465–480, 1974.
15. Saric W.S. and Nayfeh A.H. Nonparallel stability of boundary-layer flows. Physics Fluids, 18(8), 945–950, 1975.
16. Sengupta T.K. Receptivity of a growing boundary layer to surface excitation. (Unpublished manuscript), 1990.
17. Sengupta T.K., Ballav M. and Nijhawan S. Generation of Tollmien-Schlichting waves by harmonic excitation. Physics Fluids, 6(3), 1213–1222, 1994.
18. Sengupta T.K., Kameswara Rao A. and Venkatasubbaiah K. Spatiotemporal growing wave fronts in spatially stable boundary layer. Phys. Rev. Letters, 96, 224504, 2006.
19. Sengupta T.K., Kameswara Rao A. and Venkatasubbaiah K. Spatio-temporal growth of disturbances in a boundary layer and energy based receptivity analysis. Physics Fluids, 18, 094101, 2006.
20. Seifert A. and Tumin A. Nonlinear localized distrubances in an adverse pressure gradient boundary-layer transition: Experiments and linear stability analysis. In Progress in Fluid Flow Research: Turbulence and Applied MHD, vol. 182, Prog. Astro. & Aero. (Ed.: P Zarachan) 1998.
21. Fasel H. and Konzelmann U. Non-parallel stability of a flat-plate boundary layer using the complete Navier-Stokes equations. J. Fluid Mech., 221; 331–347; 1990
22. Venkatasubbaiah K. and Sengupta T.K. Mixed convection flow past a vertical plate: Stability analysis and its direct simulation. International Journal of Thermal Sciences (2008), doi:10.1016/j.ijthermalsci.2008.03.019 (In Press)
23. Kendall, J.M. Experimental study of laminar boundary layer receptivity to a traveling pressure field. AIAA Paper 87–1257, 1987.
24. Kendall, J.M. Boundary layer receptivity to free stream turbulence. AIAA Paper 90–1504, 1990.
25. Liu X. and Rodi W. Experiments on transitional boundary layers with wake induced unsteadiness. J. Fluid Mech., 231, 229–256, 1991.
26. Lieb S.J., Wundrow D.W. and Goldstein M.E. Effect of free stream turbulence and other vortical disturbances on a laminar boundary layer. J. Fluid Mech., 380, 169–203, 1999.
27. Sengupta T.K., Wang Z.Y., Yeo, K.S. and Chattopadhyay M. Receptivity to convected vortices: bypass route. Proc. 8th Asian Cong. Fluid Mech. (Ed. E. Cui), Beijing, China. 964–968, 1999.
28. Wu X., Jacobs R.G., Hunt J.C.R. and Durbin P.A. Simulation of boundary layer tranistion induced by periodically passing wakes. J. Fluid Mech., 399, 109–153, 1999.
29. Jacobs R.G. and Durbin P.A. Simulation of bypass transition. J. Fluid Mech., 428, 185–212, 2001.

30. Sengupta T.K., Chattopadhyay M., Wang Z.Y. and Yeo K.S. By-pass mechanism of transition to turbulence. J. Fluids Struct., 16(1), 15–29, 2002.
31. Taghavi-Zenouz R., Salari M., Tabar M.M. and Omidi E., Hot-wire anemometry of transitional boundary layers exposed to different freestream turbulence intensities. Proc. IMechE vol. 222, Part G: Aerospace Engg., 347-356, 2008.
32. Sengupta T.K., De S. and Sarkar S. Vortex-induced instability of an incompressible wall-bounded shear layer. J. Fluid Mech., 493, 277–286, 2003.
33. Lim T.T., Sengupta T.K. and Chattopadhyay M. A visual study of vortex-induced subcritical instability on a flat-plate laminar boundary layer. Expts. Fluids, 37, 47–55, 2004.
34. Sengupta T.K. Fundamentals of Computational Fluid Dynamics. Hyderabad: Universities Press, 2004.
35. Sengupta T.K., Ganeriwal G. and De S. Analysis of central and upwind compact schemes. J. Comput. Phys., 192(2), 677–694, 2003.
36. Van Der Vorst H.A. Bi-CGSTAB: A fast and smoothly converging variant of Bi-CG for the solution of non-symmetric linear system. SIAM J. Sci. Stat. Comput., 13(2), 631–644, 1992.